ADVANCED MATERIALS

www.advmat.de

Greatly Enhanced Anticorrosion of Cu by Commensurate Graphene Coating

Xiaozhi Xu, Ding Yi, Zhichang Wang, Jiachen Yu, Zhihong Zhang, Ruixi Qiao, Zhanghao Sun, Zonghai Hu, Peng Gao, Hailin Peng, Zhongfan Liu, Dapeng Yu, Enge Wang, Ying Jiang,* Feng Ding,* and Kaihui Liu*

Metal corrosion is a long-lasting problem in history and ultrahigh anticorrosion is one ultimate pursuit in the metal-related industry. Graphene, in principle, can be a revolutionary material for anticorrosion due to its excellent impermeability to any molecule or ion (except for protons). However, in real applications, it is found that the metallic graphene forms an electrochemical circuit with the protected metals to accelerate the corrosion once the corrosive fluids leaks into the interface. Therefore, whether graphene can be used as an excellent anticorrosion material is under intense debate now. Here, graphene-coated Cu is employed to investigate the facet-dependent anticorrosion of metals. It is demonstrated that as-grown graphene can protect Cu(111) surface from oxidation in humid air lasting for more than 2.5 years, in sharp contrast with the accelerated oxidation of graphene-coated Cu(100) surface. Further atomic-scale characterization and ab initio calculations reveal that the strong interfacial coupling of the commensurate graphene/Cu(111) prevents H_2O diffusion into the graphene/Cu(111) interface, but the one-dimensional wrinkles formed in the incommensurate graphene on Cu(100) can facilitate the H_2O diffusion at the interface. This study resolves the contradiction on the anticorrosion capacity of graphene and opens a new opportunity for ultrahigh metal anticorrosion through commensurate graphene coating.

Dr. X. Z. Xu, J. C. Yu, Z. H. Zhang, R. X. Qiao, Z. H. Sun, Prof. D. P. Yu, Prof. K. H. Liu
State Key Laboratory for Mesoscopic Physics
School of Physics
Peking University
Beijing 100871, China
E-mail: khliu@pku.edu.cn

Dr. X. Z. Xu, Z. H. Zhang, Prof. K. H. Liu
Academy for Advanced Interdisciplinary Studies
Peking University
Beijing 100871, China

Dr. D. Yi, Prof. F. Ding
Centre for Multidimensional Carbon Materials
Institute for Basic Science
Ulsan 44919, Republic of Korea
E-mail: f.ding@unist.ac.kr

Z. C. Wang, Prof. E. G. Wang, Prof. Y. Jiang, Prof. K. H. Liu
International Centre for Quantum Materials
Peking University
Beijing 100871, China
E-mail: yjiang@pku.edu.cn

Prof. Z. H. Hu
School of Electronic Engineering
Beijing University of Posts and Telecommunications
Beijing 100876, China

Prof. P. Gao
Electron Microscopy Laboratory
School of Physics
Peking University
Beijing 100871, China

Prof. P. Gao, Prof. D. P. Yu, Prof. E. G. Wang, Prof. Y. Jiang, Prof. K. H. Liu
Collaborative Innovation Centre of Quantum Matter
Beijing 100871, China

Prof. H. L. Peng, Prof. Z. F. Liu
Centre for Nanochemistry
College of Chemistry and Molecular Engineering
Peking University
Beijing 100871, China

Prof. D. P. Yu
Department of Physics
South University of Science and Technology of China
Shenzhen 518055, China

Prof. F. Ding
School of Materials Science and Engineering
Ulsan National Institute of Science and Technology (UNIST)
Ulsan 44919, Republic of Korea

Prof. K. H. Liu
Institute of Ocean Research
Peking University
Beijing 100871, China

1702944 (1 of 7)

Metal corrosion degrades metallic materials and their structures, which leads to huge financial losses.[1,2] Conventional anticorrosion methods, such as protective coating or sacrificial anode, suffer the short-term functionality (usually less than 5 years) and require very thick coating materials (from 0.01 to a few mms). Therefore, long-term and thin-layer anticorrosion coating has long been the pursuit in the modern industry and great efforts have been dedicated to this engineering direction.[3–5] In principle, a good anticorrosive material should satisfy two requirements: (i) it can prevent vertical penetration of the corrosive fluids onto the metal surface and (ii) once the corrosive fluids reach the metal surface, it can prevent the in-plane diffusion into the interface between metals and protective materials. The first requirement isolates the metal from corrosive environment and the second one restrains the corrosive damage within a small area in case the isolation is failed. Finding new anticorrosion materials which meet both requirements is of central importance in the development of anticorrosion technology.

The rise of graphene, a monolayer of hexagonal carbon atoms, opens a new opportunity for anticorrosion. Graphene satisfies requirement (i) very nicely. Due to the dense delocalized 2D electronic states, graphene shows perfect impermeability to any atom or molecule under ambient conditions,[6–9] which could in principle completely prevent contact between the metal and the corrosive environment. In addition, its chemical stability,[10] negligible thickness and weight, high thermal conductivity,[11] unparalleled mechanical strength,[12] and great optical transparency[13] can wonderfully maintain the physical properties of metals being protected, including the thickness, appearance, optical properties, electrical, and thermal conductivities. This makes graphene a very promising candidate for the ultrahigh anticorrosion materials.[14–19] However, in a large-area graphene film, the point defects and/or grain boundaries might be inevitable[20,21] and, from which, the corrosive fluids may vertically penetrate onto the metal surface.[22] Besides, graphene is a semi-metallic material and will form a battery circuit at the graphene–metal interface and therefore, a graphene coating may accelerate the electrochemical corrosion, as observed in many experiments.[23–26] So far, if graphene can be used as an effective material for anticorrosion is under high debate.

In this work, we choose Gr/Cu (graphene grown on Cu surface) as a model system to investigate the facet-dependent anticorrosion properties of graphene coating. We demonstrate that in commensurate Gr/Cu(111), H_2O will not diffuse into the interface and graphene satisfies anticorrosion requirement (ii) nicely; while in incommensurate Gr/Cu(100), H_2O can easily diffuse into the interface and accelerate the corrosion. The atomically resolved structural characterizations, together with the first-principles calculations, further reveal that the facet-dependent anticorrosion behavior is attributed to the difference of interfacial coupling between the commensurate and incommensurate Gr/Cu systems. Our results provide a new opportunity and hope for ultrahigh anticorrosion of metal by graphene coating through accurate interfacial engineering.

In our experiment, individual single-crystal graphene domains were grown on Cu(111) and Cu(100) faceted Cu foils by chemical vapor deposition (CVD) method (see the Experimental Section for growth details). Convenient optical imaging method was employed to qualitatively monitor the oxidation of Cu surface via colour change.[14] We first tested the in-plane diffusion of O_2 by putting the Gr/Cu samples in dry air (H_2O relative humidity <2%) under 50 °C for 4 h, and the results showed that in both Gr/Cu(111) and Gr/Cu(100) systems graphene protects Cu very well (**Figure 1**a; Figure S1, Supporting Information). The in-plane O_2 diffusion at the graphene–Cu interface is very slow and the anticorrosion requirement (ii) is therefore satisfied for O_2-only environment.

However, the two systems show totally different anticorrosion behaviors when H_2O is present in the environment. As for Gr/Cu(100) system, the Cu surface under graphene is heavily oxidized no matter under 50 °C for 4 h with water vapor (H_2O relative humidity >80%) (Figure 1b; Figure S2, Supporting Information) or under ≈22 °C in air for one year in Beijing (average H_2O relative humidity is ≈50% in summer and sometimes 90% in the wet weather) (Figure 1c). Auger electron spectrum proves the existence of copper oxides (Figure S3, Supporting Information) and Raman spectrum (Figure 1d) reveals that the oxide is mainly Cu_2O.[27] Time evolution data of the oxidation process show that the oxidation starts when the corrosive molecules diffuse into the interface between graphene and Cu(100) surface from the graphene edge, and then extends to the central area gradually under the humid condition (Figure S4, Supporting Information). Therefore, the requirement (ii) is poorly satisfied. Especially, under ambient conditions, the Cu oxidation is even enhanced in the area with graphene coating (Figure 1c; Figure S5, Supporting Information). In sharp contrast, in Gr/Cu(111) system, graphene can nicely protect the underneath Cu from oxidation with negligible corrosion either under 50 °C for 4 h with water vapor (Figure 1e) or under ≈22 °C in air for 2.5 years (Figure 1f). Therefore in Gr/Cu(111) system, the requirement (ii) is nicely satisfied and the diffusion of corrosive H_2O (and O_2) into the interface is significantly stopped.

To understand the mechanism of the facet-dependent oxidation behavior with the presence of H_2O, we first characterized the lattice structure of Gr/Cu(111) and Gr/Cu(100) systems by low energy electron diffraction (LEED). By choosing the proper electron energy, we can obtain the reciprocal space information of graphene and Cu surface, respectively. For Gr/Cu(111) system, the LEED patterns of graphene and Cu(111) are of the same direction (**Figure 2**a,b), which reveals that the C_{6V}-symmetry graphene lattice is well-aligned on the C_{3V}-symmetry Cu(111) surface. Indeed, graphene and Cu(111) surface have only ≈4% lattice mismatch and graphene would epitaxially grow on the Cu(111) surface to form a commensurate system (Figure 2c). But for Gr/Cu(100) system, graphene lattice does not align well with any lattice direction of Cu(100) surface and a small relative rotation is always observed (Figure 2d,e). As a matter of fact, the C_{6V}-symmetric graphene lattice could never match with the C_{4V}-symmetric Cu(100) lattice from symmetry consideration, and they thus always form an incommensurate system (Figure 2f).

We further carried out scanning tunnelling microscopy (STM) characterization to investigate the atomic-scale real-space configurations of these two systems. As for Gr/Cu(111) system, a hexagonal Moiré pattern with a periodicity of 6.6 nm was observed in the STM topography image (**Figure 3**a), which
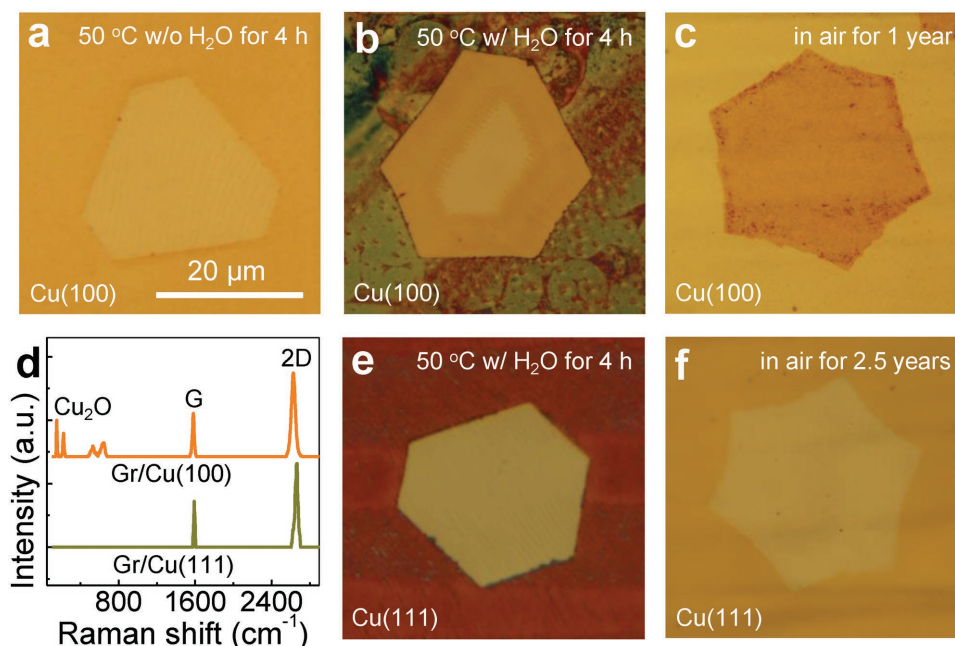
1702944 (2 of 7)

Figure 1. Facet-dependent oxidation of Cu coated by graphene. a–c) Optical images of graphene-coated Cu(100) after oxidation in dry air under 50 °C for 4 h (a), under 50 °C for 4 h with water vapor (b), and under ≈22 °C in air for one year in Beijing (c), respectively. In Gr/Cu(100), requirement (ii) is poorly satisfied at the presence of H_2O and the corrosive H_2O will easily leak into the Gr/Cu interface. d) Raman spectra of Gr/Cu(100) and Gr/Cu(111), corroborating that mainly Cu_2O forms on Cu(100) surface, while not on Cu(111). e,f) Optical images of graphene-coated Cu(111) after oxidation under 50 °C for 4 h with water vapor (e) and under ≈22 °C in air for 2.5 years (f). In Gr/Cu(111) system, the requirement (ii) is nicely satisfied and the leakage of corrosive H_2O (and O_2) into the interface is largely prevented. Image size is the same for (a–c, e–f).
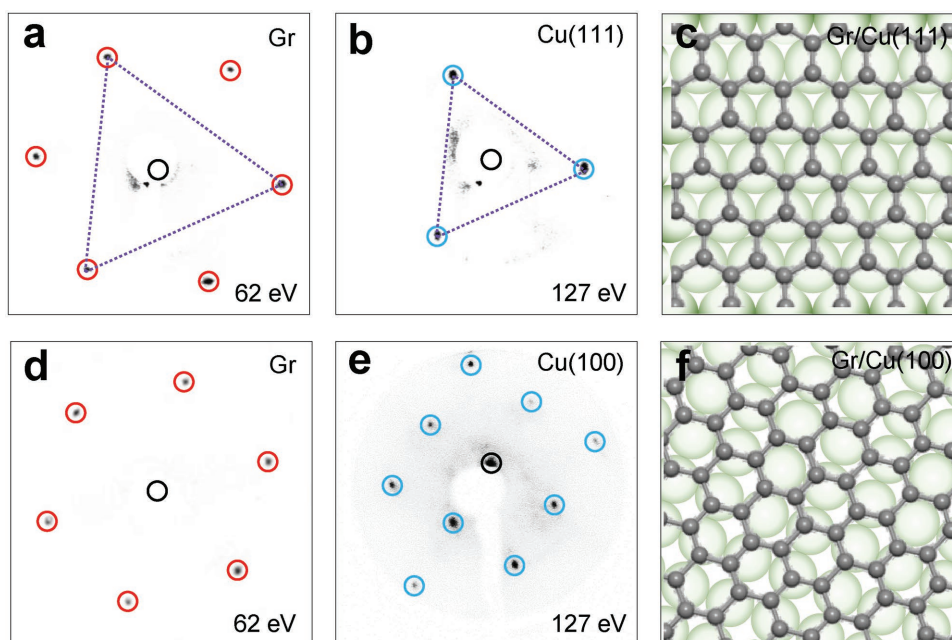

Figure 2. Reciprocal-space surface configuration in Gr/Cu systems. a,b) LEED patterns of graphene and the Cu(111) underneath obtained under different electron energies. The identical crystalline direction of graphene and Cu(111) demonstrates the epitaxial graphene growth. c) Schematic diagram of graphene lattice on Cu(111). Carbon atoms are well matched with Cu. d,e) LEED patterns of graphene and the Cu(100) underneath obtained under different electron energies. Graphene lattice shows a twist angle with Cu(100). f) Schematic diagram of graphene lattice on Cu(100). Carbon atoms cannot match with Cu. Gray (green) balls denote carbon (Cu) atoms in (c) and (f).
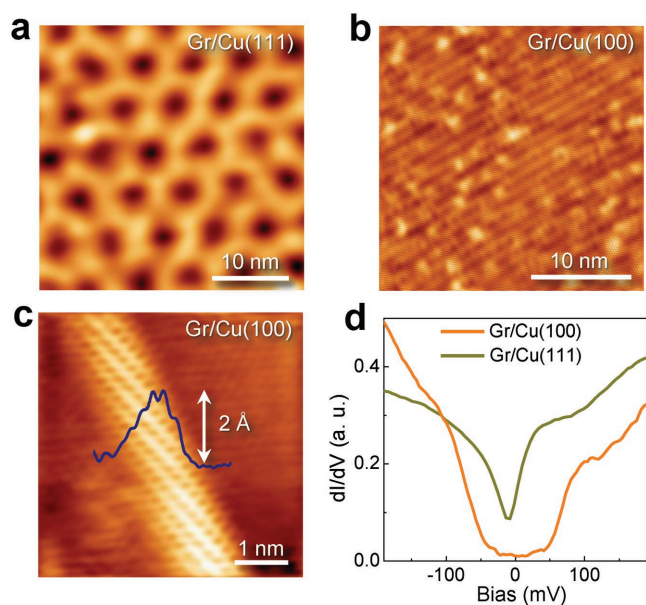
**ADVANCED
SCIENCE NEWS**

www.advancedsciencenews.com

**ADVANCED
MATERIALS**

www.advmat.de

Figure 3. Real-space surface configuration and interfacial coupling in Gr/Cu systems. a,b) STM topography of graphene on Cu(111) and Cu(100), respectively, showing two distinct surface configurations. A clear hexagonal Moiré pattern was observed on graphene/Cu(111) surface. On Cu(100), the Moiré pattern appears as 1D rows. c) STM topography of a 1D graphene wrinkle on Cu(100). The line profile of the 1D wrinkle is superimposed on the image, indicating that its height is about 2 Å. Set points of the STM images: (a) 4 V, 5 pA; (b) 0.3V, 100 pA; (c) 0.1 V, 100 pA. d) dI/dV spectra of these two configurations. A clear gap-like feature can be observed on graphene/Cu(100), while this feature is absent on graphene/Cu(111). Set point of dI/dV spectra: 0.5 V and 100 pA.

is consistent with the fact that graphene is epitaxially grown on Cu(111) surface with 4% lattice mismatch.[28] In the case of Gr/Cu(100) system, we find a periodic line-shape feature (overlapping of a C_6 symmetric graphene lattice with a C_4 one gives C_2 symmetry or a 1D Moiré pattern) (Figure 3b; Figure S6, Supporting Information). Further STM measurements on more positions show that 1D wrinkles randomly exist in the Gr/Cu(100) system. The height of this wrinkle is typically around 2 Å with respect to the flat graphene surface (Figure 3c). The formation of this 1D wrinkle should be attributed to the fact that during the cooling process after graphene growth (from 1000 to 20 °C), graphene and Cu have significantly different thermal expansion coefficients.[29] Such 1D wrinkles have never been observed in Gr/Cu(111) system, which can be understood considering the fact that it forms a hexagonal Moiré pattern and the relative strain in graphene can be released or stored due to the strong coupling between the graphene and Cu(111) surface.[30]

Scanning tunnelling spectroscopy (STS) was also conducted to study the interfacial coupling strength in the two systems. For Gr/Cu(100), we observed an ≈130 meV gap-like feature at the Fermi level, which arises from phonon-mediated inelastic electron tunnelling to graphene[31] (Figure 3d). Such a phonon-related gap can only be observed in the (nearly) freestanding graphene sample and reveals that the interfacial coupling between graphene and Cu(100) surface must be weak. But in Gr/Cu(111), this intrinsic phonon bandgap disappears,

implying a strong interfacial electronic coupling.[32] In addition, the local density of states (LDOS, proportional to dI/dV value) at charge neutral point is also higher (Figure 3d), further supporting the strong interfacial coupling between graphene and Cu(111) surface (strong interfacial coupling leads to electronic states hybridization between graphene and Cu and therefore higher LDOS).

Based on the above experimental observations, we can now qualitatively understand the facet-dependent anticorrosion behavior. In Gr/Cu(111), the graphene and the metal surface are strongly coupled and the formation of hexagonal Moiré pattern makes it resist the diffusion of H_2O into the interface. But in Gr/Cu(100), the weak interfacial interaction leads to the formation of the graphene wrinkles, which facilitate H_2O diffusion into the interface easily. Once H_2O enters the wrinkle, electrochemical reaction will happen to induce copper oxide and further enhance the corrosion (copper oxide has larger volume than Cu and induces more gaps at the interfaces for H_2O diffusion).[26,27] This facet-dependent graphene–Cu interfacial configuration is the key to determine the anticorrosion behavior.

To quantitatively understand the mechanism for the facet-dependent anticorrosion behavior, we carried out density functional theory calculations to investigate the two Gr/Cu systems (see the Supporting Information for details). As we have mentioned above, Cu and graphene have opposite-signed thermal expansion coefficients (Cu: ≈1.7×10^{-5} K^{-1}, graphene: -7×10^{-6} K^{-1} at room temperature). Considering the cooling procedure from 1000 to 20 °C in our CVD growth, we introduce a −2% relative uniaxial strain in our models (Figure S7, Supporting Information). The variations of total energy with respect to the height of wrinkles for two systems are shown in **Figure 4**a,b. It is clearly shown that a wrinkle of graphene on Cu(111) surface tends to flatten out and disappear eventually because of the strong coupling between the Cu(111) and the graphene (Figure 4a), which is in sharp contrast to what happened on Cu(100) surface, where a wrinkle formation corresponds to the global minimum of the potential energy surface due to the delicate balance between the interfacial coupling and the strain energy (Figure 4b). The optimized wrinkle height relative to the graphene surface is around ≈2.1 Å, in very good agreement with our STM result (Figure 3c).

In order to further quantitatively reveal the effect of wrinkles on the diffusion of H_2O, we further calculated the formation energies of a H_2O molecule in a series of Gr/Cu configurations (see Section S1 in the Supporting Information for details), and the corresponding structures are shown in Figure 4c,d. For flat graphene-covered Cu(111) and (100) surface (Figure 4c,d), as there is no enough space for a H_2O molecule to diffuse into the interface, an obvious bulge emerged on graphene leads to positive formation energies for both configurations. Therefore, the diffusion of H_2O into the interface between flat graphene and Cu surface is forbidden. But, if there is a wrinkle in the graphene, the formation energy of a H_2O molecule in the wrinkle (Figure 4f) becomes lower than that on bare Cu(100) surface (Figure 4e), which indicates that the 1D wrinkle can facilitate the H_2O diffusion into the graphene–Cu interface (also for O_2 shown in Figure S8,
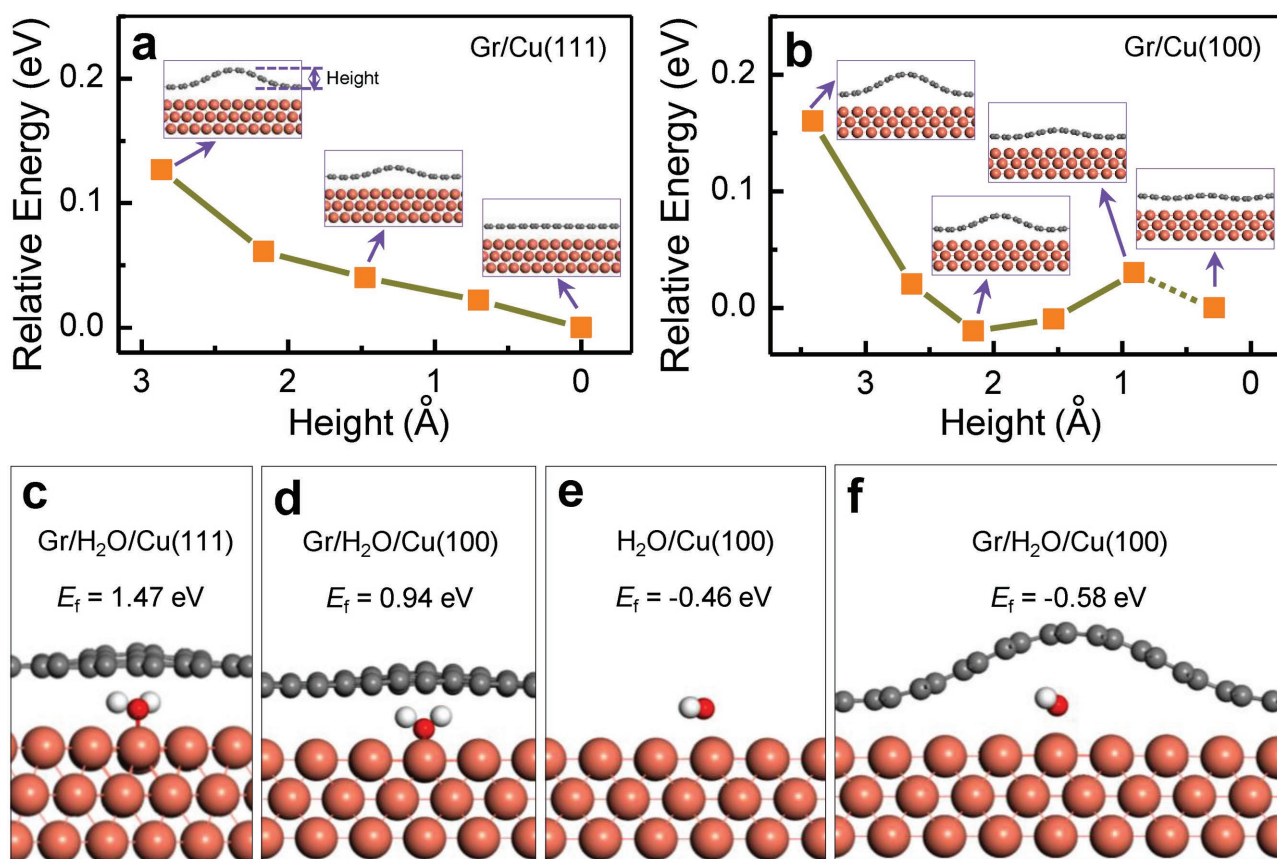
Figure 4. Theoretical simulations on the formation of wrinkles and H_2O molecules adsorption of graphene-coated Cu surfaces. a,b) Relative energy of Gr/Cu(111) and Cu(100) with respect to the height of wrinkles (defined as the distance from flat part of graphene to the peak of the wrinkles). In Gr/Cu(111) a wrinkle of graphene on Cu(111) surface tends to gradually disappear eventually, while in Gr/Cu(100) a wrinkle corresponding the global minimum of the potential energy surface can form. The data connected by solid lines mean the variation are continuous, and the rightmost data points correspond to configurations with −2% uniform strain, and are set as the references. c,d) Side view of flat graphene coated Cu(111) and (100) surfaces with a H_2O molecule inserted. e,f) Side view of bare and wrinkled graphene coated Cu(100) surfaces with a H_2O molecule adsorbed. The corresponding formation energies of the four configurations are also shown. Orange, grey, red, and white balls represent Cu, C, O, and H atoms, respectively.

Supporting Information). The formation energy difference, 0.12 eV, stems from the Van der Waals interaction between the H_2O molecule and the graphene wrinkle. Therefore, the acceleration of oxidation in Gr/Cu(100) in a humid environment can be attributed to the wrinkle formation on the strained graphene.

In addition, we studied this facet-dependent oxidation behavior in other Gr/Cu systems. Parallel with Gr/Cu(111), the commensurate Gr/Cu(311) shows ultrahigh anticorrosion effect of Cu in air for more than two years (Figure S9a–d, Supporting Information), while the incommensurate Cr/Cu(410) demonstrates similar behavior with Gr/Cu(100), and the Cu oxidation is enhanced due to the electrochemical corrosion (Figure S9e–h, Supporting Information).

The commensurate configuration needs the alignment of graphene and Cu lattice. So, the random orientation of graphene and Cu(111) would form incommensurate system and the ultrahigh protection will not work again.[23] On the other hand, if single-crystal graphene can be transferred onto Cu(111) with perfect alignment and the coupling between the graphene and Cu can be strong enough, the high

anticorrosion should also work. In fact, researchers have realized the accurate transfer of graphene with controlled orientation.[33] The little twist angle can be corrected automatically after proper annealing.[34,35] Our work provides the concept demonstration and it can be a very important direction to test the massive application in the future by transferring techniques.

The discovery and understanding of facet-dependent oxidation behavior in Gr/Cu systems is very important for the development of highly effective anticorrosion materials and technologies. Our results show that by choosing metal (111) or (311) surface to coat with graphene into a commensurate system, the graphene can satisfy both requirements in ultrahigh anticorrosion. Recently graphene single-crystal size reaches inch scale and is becoming larger and larger.[36] At the same time, it is also possible now to transform polycrystalline Cu into single crystalline Cu(111) by proper annealing technique and directly grow commensurate graphene on it.[37–39] The large-scale application of graphene coating on metal surfaces, especially Cu, Ni, or Fe, as a long-term anticorrosion technique is therefore very promising in the near future.

Experimental Section

Growth of Graphene Samples on Cu(100) and Cu(111): Graphene samples were grown by CVD method. Cu(100) and Cu(111) single crystals (Figure S3a,b, Supporting Information) annealed from Cu foils[34,35] (25 μm thick, 99.8%, Alfa Aesar) were placed on a flat oxide substrate and then loaded into a CVD system (Hefei Kejing Company OTF1250). The system was heated to 1000 °C in 1 h with Ar (500 sccm) followed by annealing in additional H_2 (10 sccm) for 40 min. Then CH_4 gas (0.1 sccm) was introduced as carbon source for graphene growth. At last, the system was cooled down naturally with Ar (500 sccm) and H_2 (10 sccm).

Hot-Vapor-Assisted Oxidation of Cu Coated with Graphene: Graphene-coated Cu foils were fixed on the glass slides and then put on top of the water bath. The temperature of the deionized water was set to 50 °C.

Optical Measurements: Raman spectra were taken by a LabRAM HR800 system with laser excitation wavelength of 633 nm, the background was removed to make characteristic peaks clearer. Optical images were taken by an Olympus microscope (Olympus BX51).

LEED and STM Measurements: LEED was performed using Omicron LEED system in ultrahigh vacuum with base pressure below 3×10^{-7} Pa. STM experiments were performed with a combined nc-atomic force microscope (AFM)/STM system (Createc, Germany) at 5 K (dI/dV measurement) and 77 K (topography imaging) with base pressure <7×10^{-9} Pa. Electrochemically etched W-tips were cleaned by alternative annealing and sputtering before the experiments, and further by controlled field-emission and tip-crash procedures during the scanning. Before STM investigations, the samples were cleaned in situ by heating it up to 450 °C for an extended time (typically longer than 10 h). Bias voltage refers to the sample voltage with respect to the tip. All of the STM topographic images were obtained in constant-current mode. The STS dI/dV spectra were acquired using lock-in detection of the tunnelling current by adding a 5 mV$_{rms}$ modulation at 481 Hz to the sample bias.

Supporting Information

Supporting Information is available from the Wiley Online Library or from the author.

Acknowledgements

Conflict of Interest

The authors declare no conflict of interest.

Keywords

[1] H. C. H. Carpenter, *Nature* **1916**, *96*, 439.
[2] R. B. Comizzoli, R. P. Frankenthal, P. C. Milner, J. D. Sinclair, *Science* **1986**, *234*, 340.
[3] *Nature* **1952**, *169*, 603.
[4] M. J. Pryor, *Nature* **1956**, *178*, 1245.
[5] S. Bohm, *Nat. Nanotechnol.* **2014**, *9*, 741.
[6] S. P. Koenig, L. D. Wang, J. Pellegrino, J. S. Bunch, *Nat. Nanotechnol.* **2012**, *7*, 728.
[7] S. Hu, M. Lozada-Hidalgo, F. C. Wang, A. Mishchenko, F. Schedin, R. R. Nair, E. W. Hill, D. W. Boukhvalov, M. I. Katsnelson, R. A. W. Dryfe, I. V. Grigorieva, H. A. Wu, A. K. Geim, *Nature* **2014**, *516*, 227.
[8] S. P. Surwade, S. N. Smirnov, I. V. Vlassiouk, R. R. Unocic, G. M. Veith, S. Dai, S. M. Mahurin, *Nat. Nanotechnol.* **2015**, *10*, 459.
[9] J. S. Bunch, S. S. Verbridge, J. S. Alden, A. M. van der Zande, J. M. Parpia, H. G. Craighead, P. L. McEuen, *Nano Lett.* **2008**, *8*, 2458.
[10] K. S. Novoselov, V. I. Fal'ko, L. Colombo, P. R. Gellert, M. G. Schwab, K. Kim, *Nature* **2012**, *490*, 192.
[11] A. A. Balandin, *Nat. Mater.* **2011**, *10*, 569.
[12] C. Lee, X. D. Wei, J. W. Kysar, J. Hone, *Science* **2008**, *321*, 385.
[13] R. R. Nair, P. Blake, A. N. Grigorenko, K. S. Novoselov, T. J. Booth, T. Stauber, N. M. R. Peres, A. K. Geim, *Science* **2008**, *320*, 1308.
[14] S. S. Chen, L. Brown, M. Levendorf, W. W. Cai, S. Y. Ju, J. Edgeworth, X. S. Li, C. W. Magnuson, A. Velamakanni, R. D. Piner, J. Y. Kang, J. Park, R. S. Ruoff, *ACS Nano* **2011**, *5*, 1321.
[15] D. Kang, J. Y. Kwon, H. Cho, J. H. Sim, H. S. Hwang, C. S. Kim, Y. J. Kim, R. S. Ruoff, H. S. Shin, *ACS Nano* **2012**, *6*, 7763.
[16] M. Topsakal, H. Sahin, S. Ciraci, *Phys. Rev. B* **2012**, *85*, 155445.
[17] D. Prasai, J. C. Tuberquia, R. R. Harl, G. K. Jennings, K. I. Bolotin, *ACS Nano* **2012**, *6*, 1102.
[18] B. Wang, B. V. Cunning, S. Y. Park, M. Huang, J. Y. Kim, R. S. Ruoff, *ACS Nano* **2016**, *10*, 9794.
[19] Y. Su, V. G. Kravets, S. L. Wong, J. Waters, A. K. Geim, R. R. Nair, *Nat. Commun.* **2014**, *5*, 4843.
[20] P. Y. Huang, C. S. Ruiz-Vargas, A. M. van der Zande, W. S. Whitney, M. P. Levendorf, J. W. Kevek, S. Garg, J. S. Alden, C. J. Hustedt, Y. Zhu, J. Park, P. L. McEuen, D. A. Muller, *Nature* **2011**, *469*, 389.
[21] D. L. Duong, G. H. Han, S. M. Lee, F. Gunes, E. S. Kim, S. T. Kim, H. Kim, Q. H. Ta, K. P. So, S. J. Yoon, S. J. Chae, Y. W. Jo, M. H. Park, S. H. Chae, S. C. Lim, J. Y. Choi, Y. H. Lee, *Nature* **2012**, *490*, 235.
[22] X. F. Feng, S. Maier, M. Salmeron, *J. Am. Chem. Soc.* **2012**, *134*, 5662.
[23] A. Y. Lu, S. Y. Wei, C. Y. Wu, Y. Hernandez, T. Y. Chen, T. H. Liu, C. W. Pao, F. R. Chen, L. J. Li, Z. Y. Juang, *RSC Adv.* **2012**, *2*, 3008.
[24] M. Schriver, W. Regan, W. J. Gannett, A. M. Zaniewski, M. F. Crommie, A. Zettl, *ACS Nano* **2013**, *7*, 5763.
[25] F. Zhou, Z. T. Li, G. J. Shenoy, L. Li, H. T. Liu, *ACS Nano* **2013**, *7*, 6939.
[26] G. Kalita, R. Papon, S. Sharma, S. M. Shinde, R. Vishwakarma, M. Tanemura, *Carbon* **2014**, *80*, 504.
[27] X. L. Yin, Y. L. Li, F. Ke, C. F. Lin, H. B. Zhao, L. Gan, Z. T. Luo, R. G. Zhao, T. F. Heinz, Z. H. Hu, *Nano Res.* **2014**, *7*, 1613.
[28] L. Gao, J. R. Guest, N. P. Guisinger, *Nano Lett.* **2010**, *10*, 3512.
[29] W. Z. Bao, F. Miao, Z. Chen, H. Zhang, W. Y. Jang, C. Dames, C. N. Lau, *Nat. Nanotechnol.* **2009**, *4*, 562.
[30] C. R. Woods, L. Britnell, A. Eckmann, R. S. Ma, J. C. Lu, H. M. Guo, X. Lin, G. L. Yu, Y. Cao, R. V. Gorbachev, A. V. Kretinin, J. Park, L. A. Ponomarenko, M. I. Katsnelson, Y. N. Gornostyrev, K. Watanabe, T. Taniguchi, C. Casiraghi, H. J. Gao, A. K. Geim, K. S. Novoselov, *Nat. Phys.* **2014**, *10*, 451.
[31] Y. B. Zhang, V. W. Brar, F. Wang, C. Girit, Y. Yayon, M. Panlasigui, A. Zettl, M. F. Crommie, *Nat. Phys.* **2008**, *4*, 627.

**ADVANCED
SCIENCE NEWS**

www.advancedsciencenews.com

**ADVANCED
MATERIALS**

www.advmat.de

[32] L. Chen, C. C. Liu, B. J. Feng, X. Y. He, P. Cheng, Z. J. Ding, S. Meng, Y. G. Yao, K. H. Wu, *Phys. Rev. Lett.* **2012**, *109*, 056804.

[33] V. L. Nguyen, D. J. Perello, S. Lee, C. T. Nai, B. G. Shin, J. G. Kim, H. Y. Park, H. Y. Jeong, J. Zhao, Q. A. Vu, S. H. Lee, K. P. Loh, S. Y. Jeong, Y. H. Lee, *Adv. Mater.* **2016**, *28*, 8177.

[34] C. R. Woods, F. Withers, M. J. Zhu, Y. Cao, G. Yu, A. Kozikov, M. Ben Shalom, S. V. Morozov, M. M. van Wijk, A. Fasolino, M. I. Katsnelson, K. Watanabe, T. Taniguchi, A. K. Geim, A. Mishchenko, K. S. Novoselov, *Nat. Commun.* **2016**, *7*, 10800.

[35] H. Yu, Z. Z. Yang, L. J. Du, J. Zhang, J. N. Shi, W. Chen, P. Chen, M. Z. Liao, J. Zhao, J. L. Meng, G. L. Wang, J. Q. Zhu, R. Yang, D. X. Shi, L. Gu, G. Y. Zhang, *Small* **2017**, *13*, 1603005.

[36] Z. Zhang, X. Xu, L. Qiu, S. Wang, T. Wu, F. Ding, H. Peng, K. Liu, *Adv. Sci.* **2017**, *4*, 170087.

[37] L. Brown, E. B. Lochocki, J. Avila, C. J. Kim, Y. Ogawa, R. W. Havener, D. K. Kim, E. J. Monkman, D. E. Shai, H. F. I. Wei, M. P. Levendorf, M. Asensio, K. M. Shen, J. Park, *Nano Lett.* **2014**, *14*, 5706.

[38] V. L. Nguyen, B. G. Shin, D. L. Duong, S. T. Kim, D. Perello, Y. J. Lim, Q. H. Yuan, F. Ding, H. Y. Jeong, H. S. Shin, S. M. Lee, S. H. Chae, Q. A. Vu, S. H. Lee, Y. H. Lee, *Adv. Mater.* **2015**, *27*, 376.

[39] X. Xu, Z. Zhang, J. Dong, D. Yi, J. Niu, M. Wu, L. Lin, R. Yin, M. Li, J. Zhou, S. Wang, J. Sun, X. Duan, P. Gao, Y. Jiang, X. Wu, H. Peng, R. S. Ruoff, Z. Liu, D. Yu, E. Wang, F. Ding, K. Liu, *Sci. Bull.* **2017**, *62*, 1039.

1702944 (7 of 7)